
Hydraulic fracturing process by using a modified two-dimensional particle flow code – method and validation

Jian Zhou and Luqing Zhang*

Key Laboratory of Shale Gas and Geoengineering,
Chinese Academy of Science,
Institute of Geology and Geophysics,
Beijing, 100029, China
Email: zhoujian@mail.iggcas.ac.cn
Email: zhangluqing@mail.iggcas.ac.cn
*Corresponding author

Zhenhua Han

Key Laboratory of Shale Gas and Geoengineering,
Chinese Academy of Science,
Institute of Geology and Geophysics,
Beijing, 100029, China
and
College of Earth Science,
University of Chinese Academy of Sciences,
Beijing, 100049, China
Email: hanzhenhua13@mails.ucas.ac.cn

Abstract: Hydraulic fracturing had been proved as a very useful tool for unconventional oil and gas development, where the fracturing fluid is injected into tight reservoirs under high pressure to enhance the permeability of rock mass. Although hydraulic fracturing theory, numerical modelling, and laboratory experiments develops fast, knowledge is still limited when the geological conditions are complex. This paper presents a numerical method – particle flow code (PFC) – and validates its power for hydraulic fracturing modelling in complex conditions. Firstly, the bonded particle method (BPM) and fluid-mechanical coupling mechanism are introduced; secondly, Darcy's flow in circular particles is simulated; thirdly, a series of numerical simulations is carried out to validate its suitability for hydraulic fracturing modelling; finally, the laminated reservoir will be modelled by BPM. The modelling results show good agreement with classical analytical solution and laboratory test results, which demonstrates that the BPM is a useful and strong tool for understanding the fracturing behaviour of reservoir rocks.

Keywords: bonded particle model; modified fluid-mechanical couple mechanism; Darcy's flow; hydraulic fracturing; validation of pressure breakdown simulation.

Reference to this paper should be made as follows: Zhou, J., Zhang, L. and Han, Z. (2017) 'Hydraulic fracturing process by using a modified two-dimensional particle flow code – method and validation', *Progress in Computational Fluid Dynamics*, Vol. 17, No. 1, pp.52–62.

Biographical notes: Jian Zhou is a post-doctor in the Institute of Geology and Geophysics, Chinese Academy of Sciences. His research interests involve rock mechanics, geological engineering and numerical simulation of hydraulic fracturing. He received his Bachelor's degree in 2008 and PhD in Geological Engineering in 2013. Since 2013, he worked as a post-doctor in the Institute of Geology and Geophysics, Chinese Academy of Sciences in the area of hydraulic fracturing process of unconventional oil and gas reservoirs.

Luqing Zhang is an Associate Professor in the Institute of Geology and Geophysics, Chinese Academy of Sciences. His research interests involve rock mechanics and geological engineering. He received his Master degree in Rock Mechanics in 1998 and PhD in Geological Engineering in 2001. Since 2001, he has worked in the Institute of Geology and Geophysics, Chinese Academy of Sciences, with special attentions to deformation and failure process, and time dependent effects of rocks paid in recent years, including hydraulic fracturing induced by pressured fluids in unconventional oil and gas reservoirs.

Zhenhua Han is currently a PhD candidate in the Institute of Geology and Geophysics, Chinese Academy of Sciences, major in Geological Engineering. She received her Bachelor's degree in 2013. Since 2013, she worked in the area of hydraulic fracturing process of unconventional oil and gas reservoirs.

1 Introduction

The production of natural gas increased rapidly in recent years due to the fact that hydraulic fracturing is successfully being used in low permeability reservoir stimulation (Maxwell et al., 2002; Warpinski et al., 2005). Even though significant progress has been made in hydraulic fracturing practices (King, 2010), more details about fluid-driven fracturing processes, including the interaction between natural fractures and hydraulic fractures, fracture patterns are essential to be understood for achieving a more wide application. Since the geomaterial is opaque, it is impossible to directly observe the subsurface hydraulic-fracture geometries. The laboratory experimental research is one of available methods to investigate hydraulic fracture initiation, propagation, intersection, and geometry in geomaterials. The X-ray computer tomography technology (Jia et al., 2013; Zuo et al., 2016; Guo et al., 2016) and acoustic emission technology (Stanchits et al., 2015) have successfully been used to investigate the hydraulic fracturing process in the laboratory. However, repetitions of the kinds of laboratory works are expensive and work intensive. Numerical simulation is an alternative for analysing the propagation behaviour of hydraulic fractures in naturally fractured reservoirs.

In the past decades, lots of models have been developed to simulate fluid-driven complex fracture networks in subsurface formation. However, this kind of simulation is still a challenging problem because the complex coupling mechanisms between fluid and solid (Yang et al., 2016), heterogeneity of reservoirs, and changing boundary conditions have to be taken into account. To simplify the research problem, the Perkins-Kern-Nordgren (PKN) model (Perkins and Kern, 1961; Nordgren, 1972) and the Khristianovic-Geertsma-de-Klerk (KGD) model (Khristianovic and Zheltov, 1955; Geertsma and De Klerk, 1969) have been developed under the assumption that the reservoir is a homogeneous, isotropic, linear elastic continuum and the fracture geometry is planar. With the development of computing power of computers, the interaction between natural fracture and hydraulic fracture in geomechanics-reservoir models was studied. McClure (2012) investigated the fracture propagation in a pre-existing discrete fracture network based on two-dimensional displacement discontinuous method (DDM). Wu and Olson (2013), using the modified 2D-DDM approach, studied the influence of stress shadow on the fracture extending pattern when considering several perforation clusters generated in a horizontal well. Chen (2012) used the commercial finite element code, ABAQUS, where the stress intensity model is replaced by a cohesive-zone fracture tip model, to simulate fracture

propagation driven by fluid, and their modelling results are in good agreement with the 2D PKN and KGD solutions. Wang (2015) also used an ABAQUS embedded extended finite element method and cohesive zone method to model fracture initiation and propagation in different brittle rocks, and the results show that fluid pressure field and fracture geometry are significantly affected by the rock in-elastic deformations.

In recent years, the discrete element method (DEM) (Cundall, 1971) has been developed to investigate hydraulic fracture growth in naturally fractured reservoirs. In DEM, the model represents an assemblage of deformable blocks or rigid particles, which are in contact and connected by bonds to represent continuum. Compared with continuum methods, such as FEM, the principle character of DEM is that the blocks or particles can break if the bond reaches its strength, and that they can contact each other again. Thus, DEM is a more natural way for modelling fracture initiation, propagation, intersection and coalescence under complex stress conditions. The particle flow code (PFC) is a typical DEM based on the bonded particle method (BPM) (Potyondy and Cundall, 2004), where the model is composed of an assemblage of bonded circular particles, whereas the complex empirical constitutive model can be substituted by a simple contact logic.

In recent years, PFC has been widely applied in geomechanics to model failure processes of geomaterials (Zhang and Wong, 2012; Li et al., 2012), and hydraulic fracturing (Hazzard et al., 2002; Al-Busaidi et al., 2005). Through comparison with results of the geometry of hydraulic fractures from laboratory experiments and field observations of microseismic locations, magnitudes and source mechanisms, Zhao and Young (2011) validated the PFC^{2D} discrete element approach for modelling hydraulic fracturing. Shimizu et al. (2011) conducted a series of hydraulic fracturing simulations in competent rock by using flow-mechanically coupled PFC^{2D} code, and investigated the influence of the particle size distribution and fluid viscosity. Their results show that in hydraulic fracturing processes the generation of tensile cracks is dominating, while the energy from shear type acoustic emission is larger than from the tensile type. After fracture creation, the velocity of fluid infiltrating into the fracture highly depends on the viscosity of the fluid. Eshiet et al. (2013) employed PFC^{2D} to model the pressure development and the subsequent fracturing and/or cavity propagation of bulk rock and sand, respectively, considering fluid flow based on the Navier-Stokes equation of an incompressible fluid with contact density. Yoon et al. (2015a, 2015b) investigated the fluid injection-induced seismicity in a reservoir for developing an enhanced geothermal system in deep underground using discrete element modelling.

Although the BPM method was used in hydraulic fracturing studies in recent years, several details about fluid-mechanical coupling in PFC^{2D} need to be modified and validated. In this article, our study focuses on validating the modified code for simulation of hydraulic fracture initiation and propagation by a particle assembled model. Firstly, the BPM and fluid-mechanical coupling mechanism are introduced; secondly, Darcy's flow in circular particles is simulated; thirdly, compared to the analytical solution of the breakdown pressure, a series of numerical simulations is carried out to validate its suitability for hydraulic fracturing modelling; and finally, a laminated reservoir is modelled by BPM.

2 Modelling method introduction

2.1 Particle flow code

Based on the DEM scheme, PFC models the interaction and the progressive movement of solid materials treated as bonded circular particles, as was described by Cundall and Strack (1979). In this article, we modified the code written by Hazzard et al. (2002) in order to validate its power of simulation of hydraulic fracturing in heterogeneous reservoir. From the manuals (Itasca Consulting Group Inc., 2008), the details of the fundamental DEM algorithm can be found, so only a summary of the bonded particle model in PFC^{2D} code will be presented here.

Although the PFC^{2D} code is based on a discontinuum model, it can also be applied to simulate the deformation characteristics of the continuum by generating bonds between circular particles (see Figure 1). The intact rock specimen is simulated as a dense packing of small circular particles, which are bonded to their neighbours by normal and shear springs at the contact points. The parallel bond model is commonly used in recent research. In this model, the increments of normal force ΔF_i^n , the tangential force ΔF_i^s and the moment ΔM can be calculated from the relative motion of particles, and they are given by

$$\Delta F_i^n = (-k^n A \Delta U^n) n_i \quad (1)$$

$$\Delta F_i^s = -k^s A \Delta U_i^s \quad (2)$$

$$\Delta M = -k^n I \Delta \theta \text{ with } \Delta \theta = (\omega^{[B]} - \omega^{[A]}) \Delta t \quad (3)$$

where k^n and k^s represent the normal and shear stiffness respectively; ΔU^n and ΔU_i^s are the increments of normal displacement and shear displacement in a timestep respectively; $\omega^{[A]}$ and $\omega^{[B]}$ are the rotation velocities of two bonded particles respectively; n_i is the normal vector of each contact ($i = 1$ or 2); Δt is the timestep; A is the cross-sectional area of the bond, and I is the moment of inertia of the bond. The new force and moment associated with parallel bond are calculated by summing the old value existing at the start of the timestep with the increments, and they are given by

$$F_i^n(t + \Delta t) = F_i^n(t) n_i + \Delta F_i^n \text{ with } F_i^n = F_j^n n_j \quad (4)$$

$$F_i^s(t + \Delta t) = F_i^s(t) + \Delta F_i^s \quad (5)$$

$$M(t + \Delta t) = M(t) + \Delta M \quad (6)$$

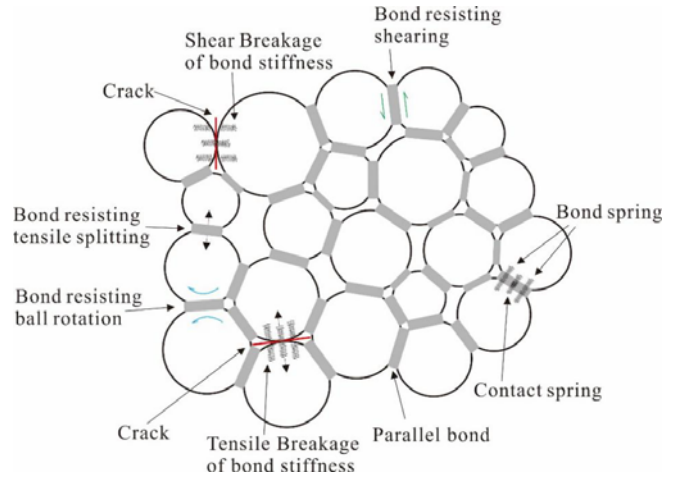
The normal stress σ and shear stress τ acting on the cross-section of the bond are calculated by the following equations. The stress is positive when the contact is in compression.

$$\sigma = \frac{-F^n}{A} + \beta \frac{|M|}{I} R \quad (7)$$

$$\tau = \frac{|F_i^s|}{A} \quad (8)$$

When σ exceeds the normal strength of bond σ_s , or τ exceeds the shear strength of bond τ_s , the bonds between the particles can break. The criterions of bond break are summarised as $|\sigma| \geq \sigma_s$ and $\sigma < 0$ (tensile stress) and $|\tau| \geq \tau_s$, respectively. They imply that the normal bond breaks only by tension, while compression does not cause the bonds to break. If a bond breaks, a micro-crack is generated at the contact point between the particles. The micro-crack length is assumed to be the same as the bond radius R , and the direction of it is perpendicular to the line joining the two centres. The crack is generated automatically under a certain failure criterion with no need for re-meshing.

Figure 1 Illustration of the parallel bond model (see online version for colours)



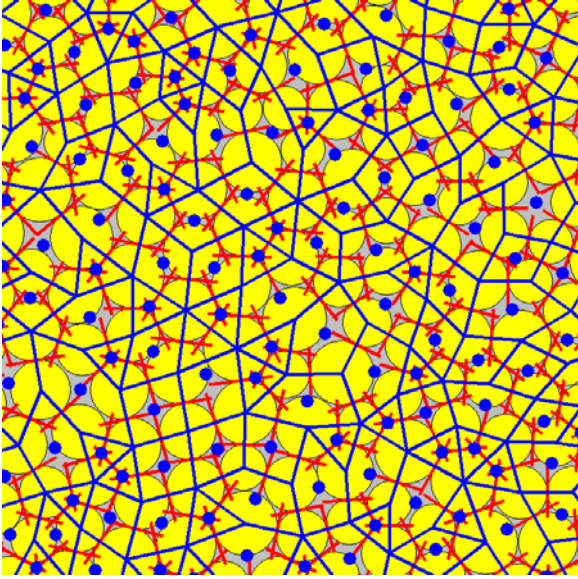
Source: Modified from Cho et al. (2007)

2.2 Mechanism of fluid-mechanical coupling in PFC^{2D}

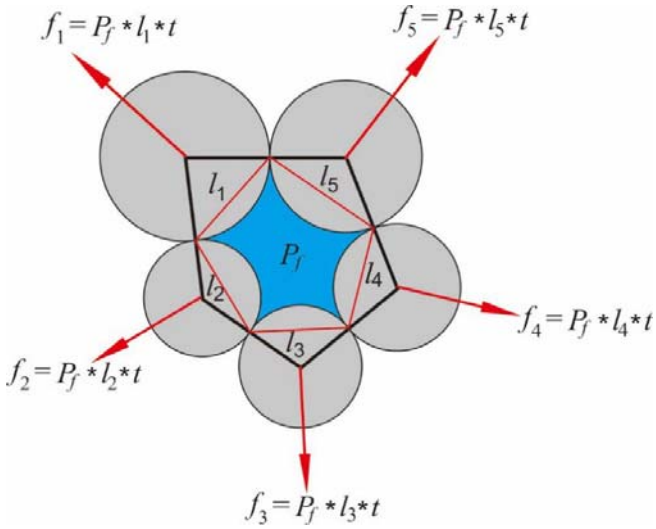
Viscous fluid flow in the BPM is simulated according to the algorithm by Cundall (2000), who proposed the original concept of a fluid flow algorithm. Cundall's fluid flow algorithm is based on two assumptions: the bond in the bonded assemblies is a flow channel (pipe), and these channels connect small reservoirs that store fluid pressure. As presented in Figure 2, the fluid network topology is formed by lines connecting the centres of all particles in

contact. The contacts generate a series of enclosed domains (Figure 2, blue polygons), whose centres are stored as a series of reservoir domains. The reservoir domains are connected by pipes (Figure 2, red lines). Each particle contact corresponds to one pipe with a length related to the two particle radii at the contact. Therefore, each reservoir is completely surrounded by contacts and has a certain volume (void space in an enclosed domain) associated with it.

Figure 2 PFC model for the fluid-mechanical simulation, (a) reservoir domains (blue polygons), the centres of domains (blue circles) and flow channels (red lines) making up the fluid network (b) mechanical coupling (see online version for colours)



(a)



(b)

Note: Red arrows are resultant forces applied to the particles surrounding the domain due to the fluid pressure P_f .

Flow of viscous fluid in each channel [Figure 2(a), red lines] is driven by the differential pressure between the two reservoir domains [Figure 2(a), blue polygons], and it is modelled using the cubic law equation, which assumes that

the flow is laminar between two smooth parallel plates. Therefore, the volumetric laminar-flow rate q is given by the following equation:

$$q = \frac{e^3 \Delta P}{12\mu L} \quad (9)$$

where e is hydraulic aperture, ΔP is the fluid pressure difference between the two neighbouring reservoir domains, L is the length of the flow channel, μ is the fluid dynamic viscosity.

During the fluid flow calculation, the increment of fluid pressure (ΔP) in a reservoir domain is computed from the bulk modulus of fluid (K_f), the volume of the domain (V_d), the sum of the flow volume for one time step (Δt) and the volume change of the domain due to mechanical loading, which is neglected in some studies (Hazzard et al., 2002; Al-Busaidi et al., 2005), but not in this article. So the equation used is given by

$$\Delta P = \frac{K_f}{V_d} \left(\sum q \Delta t - \Delta V_d \right) \quad (10)$$

Reservoir domain deformations are induced by the fluid pressure exerted on the surrounding particles [see Figure 2(b)]. This force (f) is a product of fluid pressure (P_f), the length (l) exposed to fluid in a domain and unit thickness (1 m) in out-of-plane direction. The resultant force is then applied to the particles in outward direction normal to the boundary [Figure 2(b), red polygon] which is exposed to fluid.

Figure 3 presents the modelling procedures for a fluid-mechanically coupling system in PFC^{2D}. In this figure, the modelling of mechanical deformation is shown on the left side, while the simulation of fluid migration is shown on the right side. The deformation of the reservoir causes the increase or decrease of the volume of a domain, also the hydraulic aperture of each flow channel needs to be modified according to the contact force. After the fluid calculation step, fluid pressure in the domain is exerted on the surrounding particles according to Figure 2(b).

In the present model, the fluid flow is simulated in micro-scale, where it cannot calculate the hydraulic aperture according to the deformation of bonded particles. So the hydraulic aperture of the flow channel between two particles is assumed changing as a function of normal forces. For the particles that are just touching (with 0 effective normal stress) a residual aperture, e_0 , is assumed. This ensures that fluid can still migrate, even in a model without cracks. As the normal force at a contact increases, the aperture related to force can be given as

$$e = e_{\text{inf}} + (e_0 - e_{\text{inf}}) \exp(-0.15\sigma_n) \quad (11)$$

where σ_n represents the effective normal stress at the contact (in MPa). When σ_n tends to infinity, the aperture decreases asymptotically to e_{inf} . Since flow rate q in equation (9) is the microscopic flow rate in one flow channel and the fluid flow in a rock model is expressed by an assembly of many flow channels, the permeability of the entire rock model

cannot be calculated directly from equation (9). Therefore, the values of e_0 and e_{inf} are determined according to equation (12), after Al-Busaidi et al. (2005), based on the permeability k of real rock, or by simulating the permeability test corresponding to the characteristics of an actual specimen.

$$k = \frac{1}{12V} \sum_{\text{pipes}} Le^3 \quad (12)$$

where V is the volume of the reservoir rock, and L is the length of the channel or pipe.

Specimen used in laboratory experiments or field tests are not always saturated. The fluid flow algorithm presented in Hazzard et al. (2002) and Al-Busaidi et al. (2005) employs the assumption that the entire model is always completely filled with fluid. As we know, conditions of variable saturation (dry, saturated or partially saturated) might have an influence on hydraulic fracturing, due to different fluid pressure, different distribution of microcracks, and different throughout pressure. Therefore, for taking into account the saturation conditions, a saturation factor is introduced in the fluid flow algorithm in this study. The saturation factor in each domain is defined as

$$S_t = \frac{V_f}{V_r \times \varphi} \quad (13)$$

where V_r is the volume of domain as shown in Figure 2. V_f is the volume of fluid present in the domain, and φ is the porosity of the model. Since the PFC^{2D} model is an assembly of circular particles, it is difficult to directly consider the porosity of an actual rock accurately. Therefore, the pore volume of the domain is determined by the product of the entire volume of the domain, V_r , and assumed porosity, φ .

For $S_t = 1.0$ the domain is saturated, while as $S_t < 1.0$ the domain is partially saturated. When the partially saturated

condition is considered, fluid pressure is assumed to be 0 MPa in this study in the partially saturated domain, and it increases only after the domain is saturated. In this study the initial saturation factor S_t is set to 1.0.

When the stresses caused by mechanical forces and fluid pressure in each bond exceed the tensile strength or shear strength, a microcrack starts to develop at the contact of neighbouring particles. At that time, the hydraulic aperture of the flow pipe related to the bond becomes infinite, which may cause instability in the following calculation. The simulation of fluid flow in these two domains connected by failed bond plays an important role in hydraulic fracturing in PFC. Hazzard et al. (2002), Al-Busaidi et al. (2005) and Zhao and Young (2012) think that when the bond between two domains fails, the fluid flow is instantaneous, and that the fluid pressure in these domains is assumed to be their average value P'_f before the bond failure. The calculation of the new fluid pressure is given as

$$P'_f = \frac{P_{f1} + P_{f2}}{2} \quad (14)$$

where P_{f1} and P_{f2} are fluid pressure related to domain 1 and domain 2, respectively, before the bond failure. However, equation (13) is not suitable for the condition with a well in the rock model because the volumes of some fluid domains are not approximately equal to each other. So, in this study, when the microcrack develops, the fluid pressure of two domains jointed by the failure bond is calculated by the following equation

$$P'_f = \left[\frac{(V_{f1} + V_{f2})}{(V_{r1} + V_{r2})\varphi} - 1 \right] K_f \quad (15)$$

where V_{f1} and V_{f2} are the volume of fluid existing in domain 1 and domain 2 in Figure 4, respectively, under 0 MPa fluid pressure, V_{r1} and V_{r2} are the volume of domain 1 and domain 2, respectively.

Figure 3 Modelling procedures for a fluid-mechanical coupling (see online version for colours)

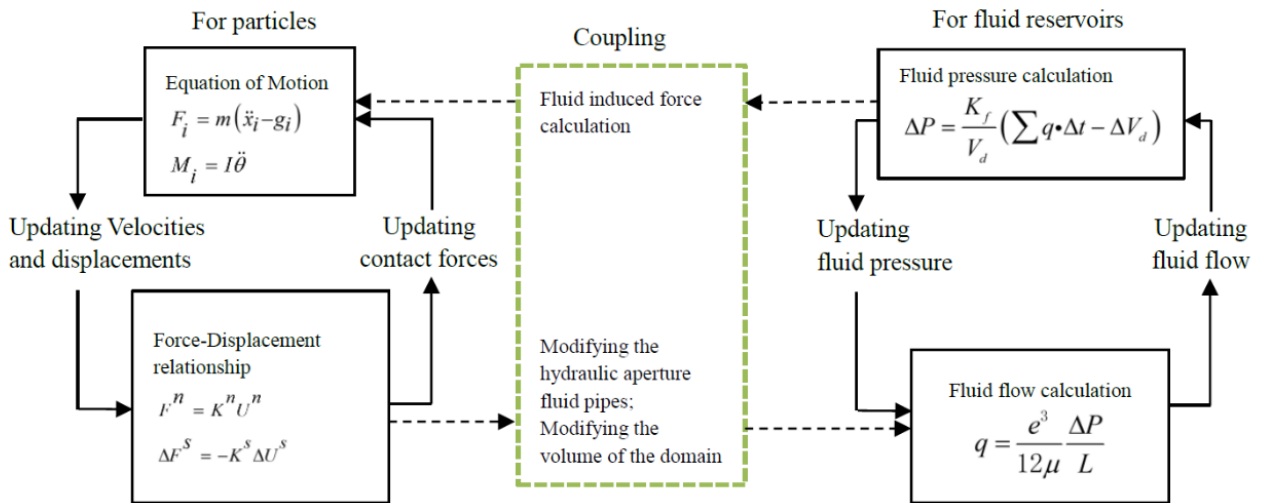
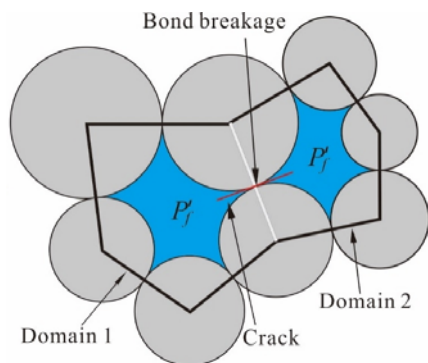


Figure 4 Bond breakage and fluid pressure balancing according to equation (15) in two related domains (see online version for colours)



3 Darcy’s flow modelling

In order to validate the fluid flow modelling by the assembled circular particles model, Darcy’s flow is simulated firstly. Figure 5(a) shows the rock specimen model represented by 1,855 bonded particles with radii from 0.2 to 0.3 m. The width and height of this model are 20 m, respectively. The upper and lower boundary of the model, indicated by the black particles in Figure 5(a), are fixed in the vertical direction, and the left and right boundaries are free. Assuming the model is saturated initially, a fluid pressure of 200 kPa is applied at the left boundary, and fluid flows in the pipes and discharges freely at the right boundary. The permeability of rock specimen is set to $1 \times 10^{-17} \text{ m}^2$, and the theoretical hydraulic aperture e is $3.46 \times 10^{-6} \text{ m}$, which is calculated according to equation (12). Figure 5(b) shows the pore-pressure field in the model after fluid infiltration more than 3.3×10^6 seconds. The fluid pressure changes from 200 kPa to 0 in horizontal direction from left to right. To reflect the fluid infiltration process, the average pore-pressure at different section positions in horizontal direction are calculated and presented in Figure 5(c) at different times. In the early stage, the pore-pressure change in horizontal direction was inhomogeneous. When fluid flow tends to be steady flow, the pore-pressure curve tends to be a line. Thus, this result shows that the DEM can be used to simulate fluid flow correctly although the model is assembled by circular particles.

4 Hydraulic fracturing modelling

4.1 Model description and parameters

The rock model and loading conditions for hydraulic fracturing are illustrated in Figure 6. The model is assembled by particles bonded with each other. The size of the rock specimen is 1,000 mm in width and 1,000 mm in height. The number of circular particles in the model is about 12,000 with particle radii ranging from 4 mm to 6 mm following a normal distribution. A borehole for viscous fluid injection with a diameter of 60 mm is created at the centre of the model. The model is surrounded by four walls,

which can move to apply the constant confining pressure to the rock model, S_H in the x-direction, and S_h in y-direction. The border of the rock model can be regarded as impermeable rubber housing. In order to create a smoothed surface within the borehole, the particles surrounding the borehole are substituted by smaller particles with half the mean radius. The macroscopic and microscopic mechanical parameters used in this study are shown in Table 1.

Figure 5 Rock specimen model for Darcy’s flow modelling and pore-pressure distribution, (a) rock specimen model (b) pore-pressure in model (c) average fluid pressure at different section position (see online version for colours)

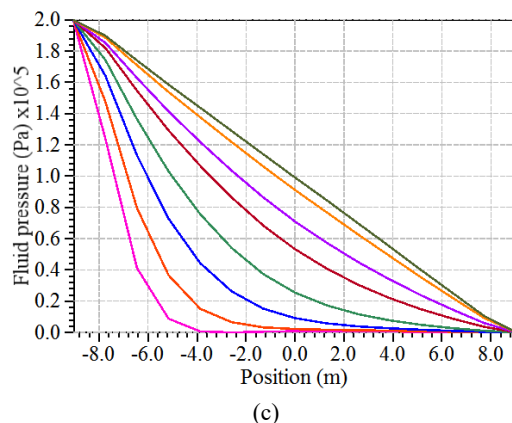
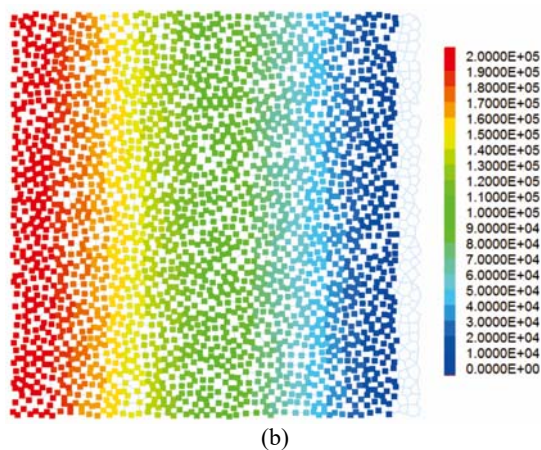
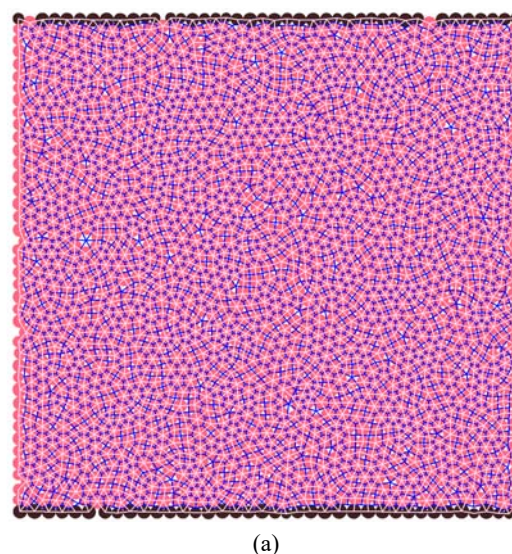
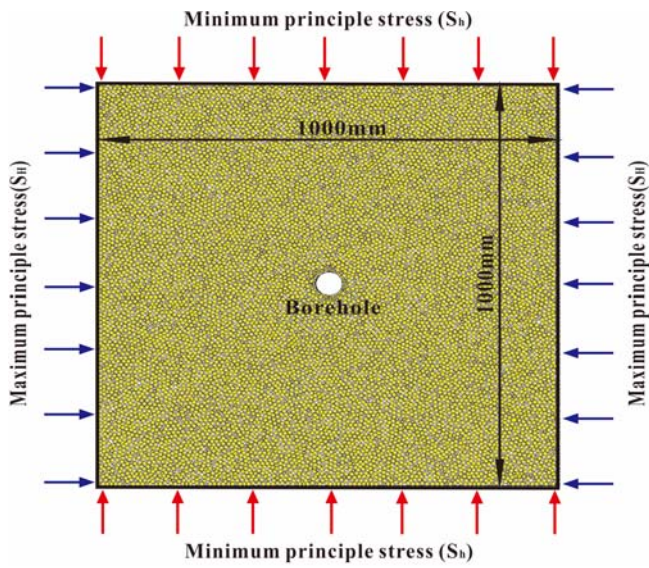


Figure 6 Rock specimen model and loading condition (see online version for colours)**Table 1** Macroscale properties of rock and microscopic input parameters

<i>Rock properties</i>		
Uniaxial compressive strength of rock (MPa)	σ_c	46.1
Tensile strength (MPa)	σ_t	4.4
Young's modulus (GPa)	E	44.2
Poisson's ratio	ν	0.20
Porosity (%)	φ	10
Permeability (m^2)	κ	1×10^{-17}
<i>Input micro-parameters</i>		
Lower bound of particle radius (mm)	R_{min}	4.0
Ratio of upper bound of particle radius to lower bound of particle radius.	R_{min}/R_{max}	1.5
Particle density (kg/m^3)	ρ	3,095
Young's modulus of the particle (GPa)	E_c	32.0
Ratio of normal to shear stiffness of the particle	k_n/k_s	1.6
Friction coefficient of particle	μ	0.30
Young's modulus of the parallel bond (GPa)	\bar{E}_c	32.0
Ratio of normal to shear stiffness of the parallel bond	\bar{k}_n/\bar{k}_s	1.6
Tensile strength of the parallel bond (MPa)	$\bar{\sigma}_t$	12.0
Cohesion of the parallel bond (MPa)	\bar{c}	30.0
Friction angle of the parallel bond ($^\circ$)	$\bar{\phi}$	45.0
Radius multiplier	$\bar{\lambda}$	1.0
Moment contribution factor	β	0.2
<i>Hydraulic properties</i>		
Initial saturation (%)	S_r	100
Initial hydraulic aperture (m)	e_0^1	2.2×10^{-6}
Infinite hydraulic aperture (m)	e_{inf}^1	2.2×10^{-7}
Bulk modulus of the fracturing fluid (GPa)	K_f	2.0

Note: ¹Calculated according to equation (12).

4.2 Validation of hydraulic fracturing model

The possibility of using the BPM to simulate fluid flow in solid materials has been identified by some researches (Hazzard et al., 2002; Al-Busaidi et al., 2005). However, for modelling hydraulic fracturing not only the fluid flow, but also crack initiation and crack propagation have to be taken into account. In past research work, the efficiency of the BPM for hydraulic fracturing simulation has been overlooked. In the work of Wang et al. (2014), the influence of the initial stress parameters and the tensile strength of a coal seam on the breakdown pressure under certain injection conditions are analysed, and a regression equation [equation (10) in Wang et al. (2014)] is obtained by fitting curves of hydraulic fracturing simulation results. This regression equation is different from the classical Kirsch equations for stress concentration around a circular elastic borehole, which have been proposed by Hubbert and Willis (1957), as following expression

$$P_{wf} = 3S_h - S_H - P_0 + \sigma_t \quad (16)$$

Figure 7 shows the idealised borehole fluid pressure response during hydraulic fracturing. The first linear part represents the elastic deformation of the system in and around the borehole, which is primarily due to compression of the injection fluid in the borehole. The peak represents the crack initial condition, and after this point the fluid pressure drops. This implies a situation of unstable crack development, and the fluid entering the voids of cracks. Continued pumping will eventually result in stable crack growth, represented by the constant borehole fluid pressure level. In this idealised case, the point of crack initiation and formation breakdown are the same, and the peak corresponds to the breakdown pressure.

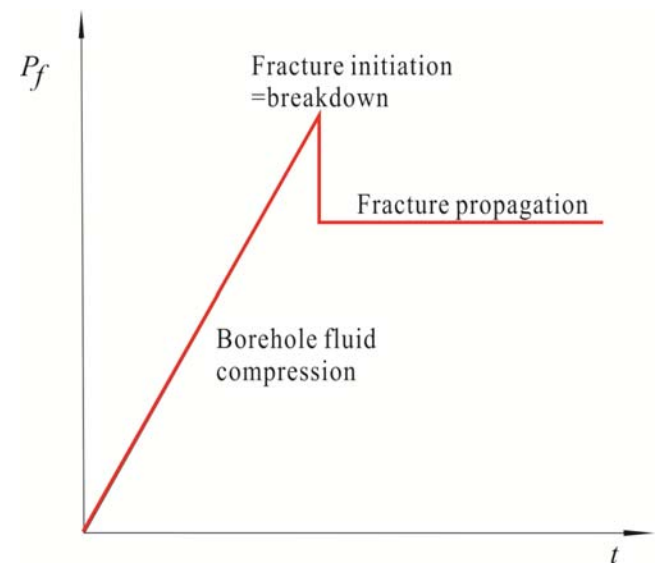
Figure 7 Idealised borehole fluid pressure response during hydraulic fracturing (see online version for colours)

Figure 8 Fluid pressure history at the injection borehole during hydraulic fracturing simulation under different confining pressures in horizontal-direction, (a) $S_H = 12.0$ MPa (b) $S_H = 13.0$ MPa (c) $S_H = 15.0$ MPa (d) $S_H = 18.0$ MPa (e) $S_H = 18.0$ MPa

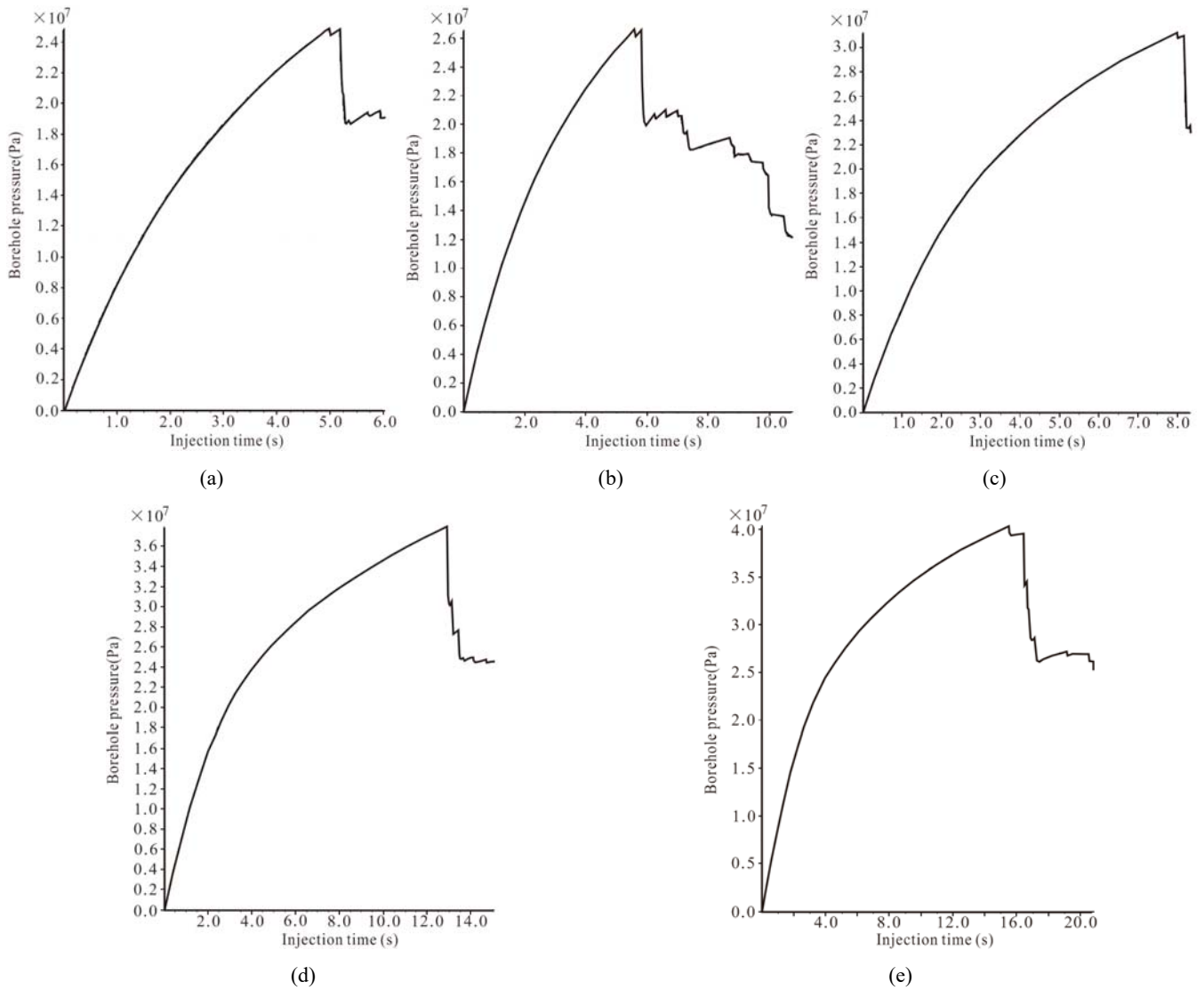
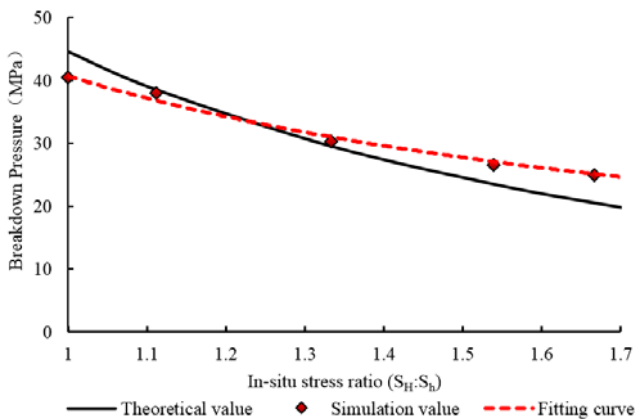


Figure 9 Breakdown pressures obtained from modelling and theoretical calculation based on equation (16) at different in-situ stress ratios (S_H/S_h) (see online version for colours)



In order to validate the reliability of hydraulic fracturing simulation by the BPM, also the influence of the in-situ

stress ratio on breakdown pressure is studied under the assumption that the initial pore-pressure is 0 ($P_0 = 0$), the dynamic viscosity of the injection fluid is $0.001 \text{ Pa}\cdot\text{s}$, and the injection rate is fixed at $2.0 \times 10^{-6} \text{ m}^3/\text{s}$. Confining pressure in x-direction (S_H) is set to 20 MPa, and the confining pressure in y-direction (S_h) changes from 20 MPa to 10 MPa. Figure 8 shows the fluid pressure history at the injection borehole during hydraulic fracturing simulation under different confining pressures in y-direction. Compared to the idealised fluid pressure history during hydraulic fracturing (Figure 7), the fluid pressure curve in Figure 8 is not linear before arriving at the breakdown pressure. This is because in PFC modelling leakage is taken into account in the algorithm design. When fluid is pumped into the borehole, it can according to the cubic law enter the neighbour domains instantaneously through the fluid pipes. Comparing the curves in Figure 8, the conclusion can be made that leakage is increasing with increasing fluid pressure. During unstable growth of hydraulic cracks the fluid pressure also drops. The breakdown pressure values

obtained from modelling and the theoretical values calculated according to equation (16) under different in-situ stress ratios are shown in Figure 9. When the ratio of S_{H1}/S_h is between 1.0 and 1.7 the error between the modelled value and the idealised analytical value is less than 20%, where the tensile strength of the rock model is 4.4 MPa. This indicates that hydraulic fracturing simulation by PFC^{2D} is able to reproduce the realistic processes to an acceptable degree.

5 Validation using laboratory UCS test of laminated reservoir rock

As we know, shale gas is stored in laminated shale reservoirs. The complexity of the mechanical properties of shale reservoirs needs to be taken into account in shale gas exploitation. When using PFC^{2D} to simulate hydraulic fracturing in shale reservoirs, the first point is to generate a numerical model, which can reflect the properties of shale rock. It is generally considered that the microscopic parameters in a PFC^{2D} model should be calibrated by comparing the results from the numerical simulation with experimental results of intact rock specimen under uniaxial compressive test (UCT) or Brazilian test. In this study, the rock specimens used for microscopic parameter calibration were from the outcrops of the Longmaxi Formation in Xiliao, Shizhu County, which is the natural extension of the formations in Pengshui shale gas block. These shale specimens are typical laminated rock with different inclination angles. After UCT, the axial and radial deformation and uniaxial strength are shown in Figure 10. The uniaxial compressive strength of the specimen with inclination angles of 0°, 30°, 45°, 60° and 90° are 159.8 MPa, 120.2 MPa, 143.1 MPa, 162.8 MPa and 168.6 MPa, respectively. Their elastic modules are between 24.6 GPa and 30.0 GPa, with the Poisson's ratio between 0.16 and 0.24.

A series of transversely isotropic rock models was constructed by embedding weak layers in the rock matrix using the BPM (Figure 11). The thickness of each layer of matrix and weak layer are approximately equal. The microscopic parameters for this transversely isotropic rock model were optimised and listed in Table 2, which will be used in the following study. Uniaxial compressive modelling results show that the UCS is consistent with the experimental results, and the average error is less than 5% (Figure 12). Also, the failure patterns of rock models from numerical modelling are consistent with failure patterns of rock specimen at different inclination angle respectively (Figure 12). For low inclination angle specimen ($\alpha = 0^\circ, 30^\circ$) under uniaxial compression, major cracks are created parallel to the direction of loading, and it is unlikely to happen that cracks develop along the bedding plane. For medium inclination angle specimen ($\alpha = 45^\circ, 60^\circ, 75^\circ$), a sudden failure occurred along the weak layer when the shear stress approached its shear strength. When $\alpha = 90^\circ$, due to no lateral confinement under uniaxial loading, a delamination failure occurred.

Figure 10 The strain-stress curves of specimen with different inclination (α) under UCT (see online version for colours)

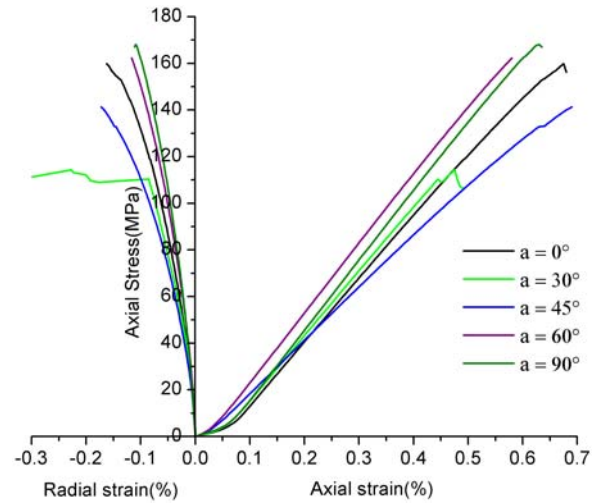
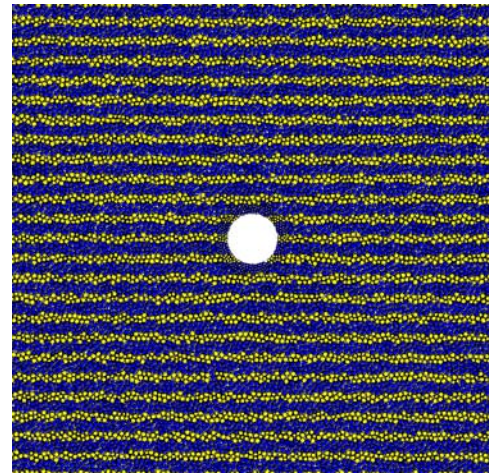


Figure 11 Numerical model of shale rock with a borehole (see online version for colours)



Note: Blue layers represent matrix, yellow layers are weak layers.

Figure 12 Comparison of UCS from laboratory tests and numerical modelling (see online version for colours)

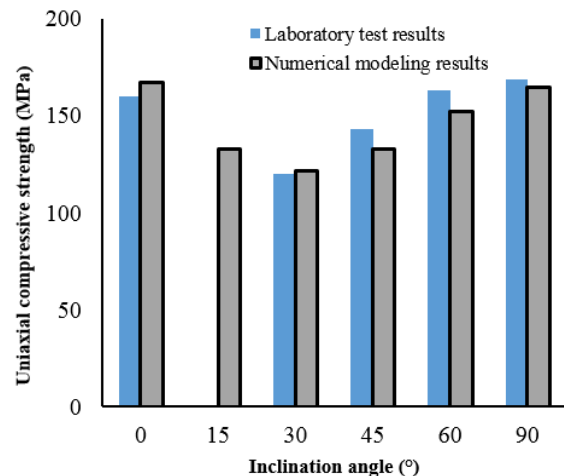
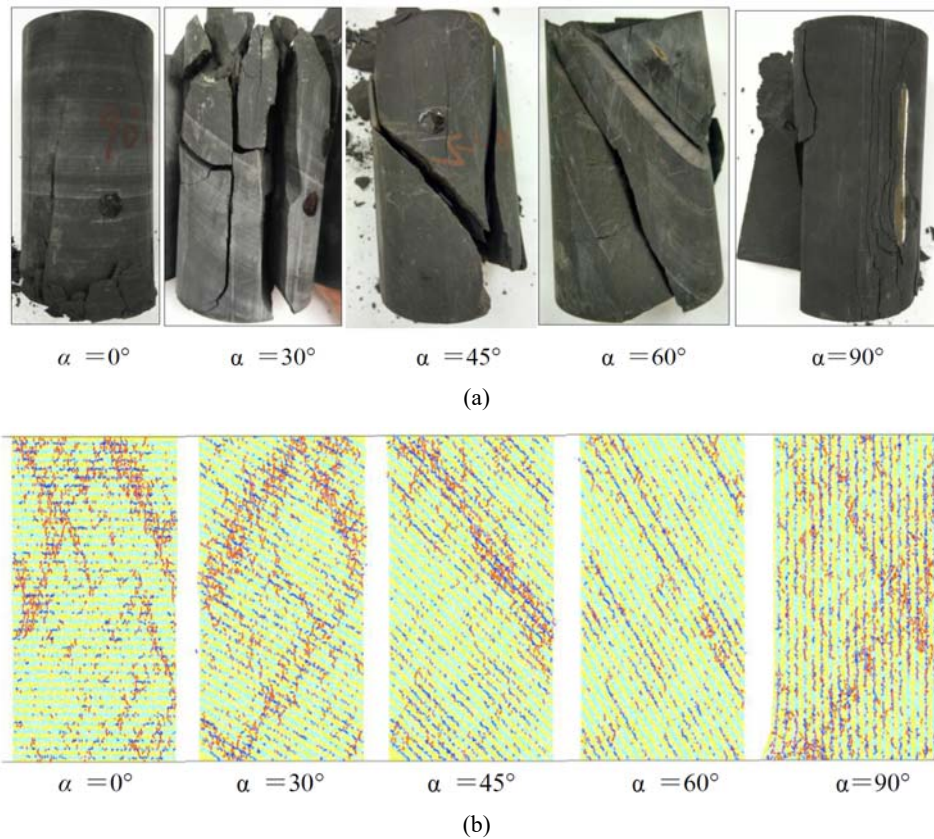


Figure 13 Failure patterns of different inclination specimen, (a) laboratory results (b) numerical simulation results (see online version for colours)



Note: Ed and blue lines representing tensile and shear cracks respectively.

Table 2 Microscopic parameters for transversely isotropic rock models

Microscopic parameters	Matrix layer	Weak layer
R_{\min} (mm)	4.0	4.0
R_{\max}/R_{\min}	1.5	1.5
ρ (kg/m ³)	3095	3095
E_c (GPa)	24.1	21.7
k_n/k_s	1.6	2.88
μ	0.7	0.30
\bar{E}_c (GPa)	24.1	21.7
\bar{k}_n / \bar{k}_s	1.6	2.88
$\bar{\sigma}_i$ (MPa)	70.0	35.0
$\bar{\tau}$ (MPa)	173.0	51.9
$\bar{\lambda}$	0.2	0.2

6 Conclusions

The DEM is available to mimic rock fracturing naturally. After the fluid-mechanical coupling mechanism is embedded, the method can be applied to fluid flow in pores and hydraulic fracturing of reservoirs. In this article, a series of simulations was performed by using a modified fluid-mechanically coupled model in PFC^{2D} to validate its power. The modelling results show good agreement with

classical analytical solutions and laboratory test results. This demonstrates that the BPM is a useful and strong tool for understanding the fracturing behaviour of reservoir rocks.

Acknowledgements

This research is supported by funding from the National Natural Science Foundation of China (Grants 41572312, 41502307, 41272353) and the Strategic Priority Research Program of the Chinese Academy of Sciences (Grants XDB10050202). The authors thank Dr. Hazzard provided his original code for hydraulic fracturing modelling. The authors thank Dr. Anika Braun for her kind help about polishing the language.

References

- Al-Busaïdi, A., Hazzard, J.F. and Young, R.P. (2005) 'Distinct element modeling of hydraulically fractured Lac du Bonnet granite', *Journal of Geophysical Research: Solid Earth*, Vol. 110, No. B6, pp.1–14.
- Chen, Z. (2012) 'Finite element modelling of viscosity-dominated hydraulic fractures', *Journal of Petroleum Science and Engineering*, Vol. 88, pp.136–144.
- Cho, N.A., Martin, C.D. and Sego, D.C. (2007) 'A clumped particle model for rock', *International Journal of Rock Mechanics and Mining Sciences*, Vol. 44, No. 7, pp.997–1010.

- Cundall, P.A. (1971) 'A computer model for simulating progressive, large-scale movements in blocky rock systems', in *Proceedings of the International Symposium on Rock Fracture*, Nancy, France, 4–6 October.
- Cundall, P.A. (2000) *Fluid Formulation for PFC^{2D}*, Itasca Consulting Group, Minneapolis, USA.
- Cundall, P.A. and Strack, O.D. (1979) 'A discrete numerical model for granular assemblies', *Geotechnique*, Vol. 29, No. 1, pp.47–65.
- Eshiet, K.I., Sheng, Y. and Ye, J. (2013) 'Microscopic modelling of the hydraulic fracturing process', *Environmental Earth Sciences*, Vol. 68, No. 4, pp.1169–1186.
- Geertsma, J. and De Klerk, F. (1969) 'A rapid method of predicting width and extent of hydraulically induced fractures', *Journal of Petroleum Technology*, Vol. 21, No. 12, pp.1571–1581.
- Guo, T., Zhang, S. et al. (2014) 'Experimental study of hydraulic fracturing for shale by stimulated reservoir volume', *Fuel*, Vol. 128, pp.373–380.
- Hazzard, J.F., Young, R.P. and Oates, S.J. (2002) 'Numerical modeling of seismicity induced by fluid injection in a fractured reservoir', in *Proceedings of the 5th North American Rock Mechanics Symposium Mining and Tunnel Innovation and Opportunity*, Toronto, ON, Canada, 7–10 July, pp.1023–1030.
- Hubbert, M.K. and Willis, D.G. (1957) 'Mechanics of hydraulic fracturing', *Transactions of Society of Petroleum Engineers of AIME*, Vol. 210, pp.153–168.
- Itasca Consulting Group Inc. (2008) *PFC^{2D} – Particle Flow Code in 2 Dimensions*, Version 4.0, Minneapolis.
- Jia, L., Chen, M., Sun, L. et al. (2013) 'Experimental study on propagation of hydraulic fracture in volcanic rocks using industrial CT technology', *Petroleum Exploration and Development*, Vol. 40, No. 3, pp.405–408.
- Khrstianovic, S. and Zheltov, Y. (1955) 'Formation of vertical fractures by means of highly viscous fluids', in *Proceedings of the 4th World Petroleum Congress*, Rome, Italy, 6–15 June, Vol. 2, pp.579–586.
- King, G.E. (2010) 'Thirty years of gas shale fracturing: what have we learned?', in *Proceedings of the SPE Annual Technical Conference and Exhibition*, Florence, Italy, 19–22 September.
- Li, W.C., Li, H.J., Dai, F.C. and Lee, L.M. (2012) 'Discrete element modeling of a rainfall-induced flowslide', *Engineering Geology*, Vol. 149, pp.22–34.
- Maxwell, S.C., Urbancic, T.I., Steinsberger, N. and Zinno, R. (2002) 'Microseismic imaging of hydraulic fracture complexity in the Barnett shale', in *SPE Annual Technical Conference and Exhibition*, Paper SPE 77440, San Antonio, Texas, 29 September–2 October.
- McClure, M.W. (2012) *Modeling and Characterization of Hydraulic Stimulation and Induced Seismicity in Geothermal and Shale Gas Reservoirs*, Doctoral dissertation, Stanford University.
- Nordgren, R.P. (1972) 'Propagation of a vertical hydraulic fracture', *Society of Petroleum Engineers Journal*, Vol. 12, No. 4, pp.306–314.
- Perkins, T.K. and Kern, L.R. (1961) 'Widths of hydraulic fractures', *Journal of Petroleum Technology*, Vol. 13, No. 9, pp.937–949.
- Potyondy, D.O. and Cundall, P.A. (2004) 'A bonded-particle model for rock', *International Journal of Rock Mechanics and Mining Sciences*, Vol. 41, No. 8, pp.1329–1364.
- Shimizu, H., Murata, S. and Ishida, T. (2011) 'The distinct element analysis for hydraulic fracturing in hard rock considering fluid viscosity and particle size distribution', *International Journal of Rock Mechanics and Mining Sciences*, Vol. 48, No. 5, pp.712–727.
- Stanchits, S., Burghardt, J. and Surdi, A. (2015) 'Hydraulic fracturing of heterogeneous rock monitored by acoustic emission', *Rock Mechanics and Rock Engineering*, Vol. 48, No. 6, pp.2513–2527.
- Wang, H. (2015) 'Numerical modeling of non-planar hydraulic fracture propagation in brittle and ductile rocks using XFEM with cohesive zone method', *Journal of Petroleum Science and Engineering*, Vol. 135, pp.127–140.
- Wang, T., Zhou, W., Chen, J., Xiao, X., Li, Y. and Zhao, X. (2014) 'Simulation of hydraulic fracturing using particle flow method and application in a coal mine', *International Journal of Coal Geology*, Vol. 121, pp.1–13.
- Warpinski, N.R., Kramm, R.C., Heinze, J.R. and Waltman, C.K. (2005) 'Comparison of single- and dual-array microseismic mapping techniques in the Barnett shale', in *SPE Annual Technical Conference and Exhibition*, Paper SPE 95568, Dallas, Texas, 9–12 October.
- Wu, K. and Olson, J.E. (2013) 'Investigation of critical in situ and injection factors in multi-frac treatments: guidelines for controlling fracture complexity', in *SPE Hydraulic Fracturing Conference*, Paper SPE 163821, Woodlands, Texas, 4–6 February.
- Yang, D., Li, Q. and Zhang, L. (2016) 'Propagation of pore pressure diffusion waves in saturated dual-porosity media (II)', *Journal of Applied Physics*, Vol. 119, No. 15, pp.154901, doi: 10.1063/1.4946832.
- Yoon, J.S., Zimmermann, G. and Zang, A. (2015a) 'Discrete element modeling of cyclic rate fluid injection at multiple locations in naturally fractured reservoirs', *International Journal of Rock Mechanics and Mining Sciences*, No. 74, pp.15–23.
- Yoon, J.S., Zimmermann, G. and Zang, A. (2015b) 'Numerical investigation on stress shadowing in fluid injection-induced fracture propagation in naturally fractured geothermal reservoirs', *Rock Mechanics and Rock Engineering*, Vol. 48, No. 4, pp.1439–1454.
- Zhang, X.P. and Wong, L.N.Y. (2012) 'Cracking processes in rock-like material containing a single flaw under uniaxial compression: a numerical study based on parallel bonded-particle model approach', *Rock Mechanics and Rock Engineering*, Vol. 45, No. 5, pp.711–737.
- Zhao, X. and Young, R.P. (2011) 'Numerical modeling of seismicity induced by fluid injection in naturally fractured reservoirs', *Geophysics*, Vol. 76, No. 6, pp.WC167–WC180.
- Zuo, Y., Zhang, S. et al. (2016) 'Experimental investigation into hydraulic fracture network propagation in gas shales using CT scanning technology', *Rock Mechanics and Rock Engineering*, Vol. 49, No. 1, pp.33–45.